



Power Conditioner Design and Control for a Grid-Connected Proton Exchange Membrane Fuel Cell

Majid Hosseinpour^{1*}, Tooraj Sabetfar², Abdolmajid Dejamkhooy³

^{1, 2, 3}Department of Electrical Engineering, University of Mohaghegh Ardabili, Ardabil, Iran
E-mail: hoseinpour.majid@uma.ac.ir

Received: October 08, 2022

Revised: November 24, 2022

Accepted: November 30, 2022

Abstract— In this paper, the design, control and stability analysis of the inverter-based power conditioner - which is connected to the low voltage grid via an LCL filter - is presented to manage the power flow of the Proton Exchange Membrane Fuel Cell (PEMFC). Since the PEMFC-generated voltage is lower than the grid voltage, a DC-DC converter is utilized to increase the PEMFC output voltage. The LCL filter is employed to improve the injected current quality and to reduce the inverter output voltage distortions. This filter can cause resonance and system instability. The current double feedback control method, which uses inverter side and grid side currents as feedback current, is suggested to dampen the resonance and improve harmonic eliminations. The suggested power conditioner system is simulated in MATLAB/Simulink to verify the model performance and the suggested control method. The obtained results show i) good performance of the suggested system in managing PEMFC power flow into the grid, ii) high quality of the injected current and iii) system stability against the grid impedance change disturbances.

Keywords— Proton exchange membrane fuel cell; LCL filter; Current double feedback; Stability analysis.

1. INTRODUCTION

Nowadays, environmental concerns such as global warming and greenhouse gas's harmful effects cause to endeavor to reduce fossil fuel consumption. Due to being clean and available, renewable energy resources such as solar energy, wind energy and fuel cells can be considered as main alternatives to fossil fuels [1, 2]. Fuel cells are electrochemical devices which convert hydrogen inner chemical energy into electrical energy. Fuel cells usually produce low voltage, and several cells are connected in series. Some advantages of fuel cells are clean production and high reliability and efficiency [3].

The three main parts of the fuel cells are the electrolyte, cathode, and anode. Fuel and oxygen enter via special channels into the cathode and the anode. Regarding electrolyte type, the cells can be divided into different categories [4]. Due to low-temperature operation, high power density, non-emission of CO₂, and fast starting, the Proton Exchange Membrane Fuel Cells (PEMFC) are adopted as Distributed Energy Resources (DER) in the distribution grids and are employed in hybrid vehicles widely [5, 6]. In large-scale fuel cell power plants, solid oxide fuel cell (SOFC) and molten carbonate fuel cell (MCFC) types are utilized because of their high efficiency and fast response to load changes [4, 7]. Grid-connected hybrid systems, which include PV and fuel cells, are attended by researchers. If the PV system does not supply

* Corresponding author

the load due to a change in irradiation or temperature, the fuel cell will compensate power lack [8, 9].

Fuel cell generated voltage is lower than the grid voltage. Therefore, it is necessary to utilize a DC-DC converter to increase the voltage level [10]. Voltage Source Inverter (VSI) converts DC voltage into AC and connects the fuel cell to the grid. So far, different control methods have been presented for connecting the fuel cells to the grid. In [11, 12], the inverter is controlled by a synchronous reference frame based on active and reactive power control. In [13], the fuel cell-inverter system uses a second-order notch filter to yield a high-quality output current.

To improve injected current quality, four types of filters, L, LC, LCL, and LLCL, are utilized as an interface between the inverter and the grid [14, 15]. In the L-type filter, an inductance reduces current harmonics. For better performance, the inductance should be large enough, or the switching frequency should be high, which causes more losses [16]. LC filter includes an inductance and a capacitor. Compared with the L filter, this filter shows better performance in the high frequencies and smaller inductance sizes. High inrush current and resonance frequency dependence on the grid impedance are the LC filter disadvantages [17]. LCL filter is constructed of a converter side inductance, a grid side inductance, and a capacitor. Compared with the L filter, the inductance size is smaller. The LCL filter's performance in eliminating high-frequency harmonics is better than other types [18]. If a small inductance connects to the capacitor of the LCL filter, the LLCL filter will be yielded. It can be utilized in high-power inverters. Compared with LCL filters, LLCL filters show more effective harmonic attenuation in the switching frequency. Similar to high-order filters, LLCL filters have resonance problems, which leads to system instability [19].

Utilizing LCL filters in the output of the inverters may cause resonance and system instability. Therefore, damping methods are necessary to ensure system stability [20, 21]. Active Damping (AD) and Passive Damping (PD) are two main approaches to damping the LCL filter resonance phenomenon. Due to smaller power loss in the AD methods, these methods are preferred. On the other hand, AD methods require voltage and current sensors and complicated control schemes. Various methods for active damping of the LCL filter resonance have been presented. The dominant method is based on capacitor voltage or current feedback. By considering calculation and PWM delays, capacitor current feedback equals virtual impedance parallel with the LCL filter capacitor [22]. Filter resonance frequency changes by virtual impedance. In LCL filters, the system stability depends on resonance frequency (f_r) and sampling frequency (f_s). In the low voltage grids, the system stability is limited to one-sixth of the sampling frequency. If $f_r < f_s/6$, the inverter side's inductance current feedback will stable the system, and the grid side's inductance current feedback cannot stable the system. If $f_r > f_s/6$, the grid side current feedback will stabilize the system [23, 24]. If the real resonance frequency is higher than one-sixth of the sampling frequency, the virtual impedance will have a negative resistive component. Then, an unstable pole pair will be yielded in the open-loop transfer function, which causes non-minimum phase behavior [25].

In this paper, PEMFC power flow into the low-voltage grid via an LCL filter enhanced inverter is investigated. To control the Grid-Connected Fuel Cell Inverter via an LCL filter (GCFCI-LCL), a current dual feedback scheme is suggested. This scheme is based on the

inverter side current and the grid side current feedback to dampen the LCL filter resonance and attenuate the voltage harmonics. Converter side Current Feedback (CCF) damps the resonance and improves the inverter side current quality. Grid side Current Feedback (GCF) maintains the system stability against the grid impedance changes. A systematic trend for the parameters design of the suggested control scheme is investigated. Resonance damping, marginal stability, and on-grid characters are considered to ensure the grid-connected system stability.

The paper is structured as follows: section 2 is about the construction and operation of the fuel cells. In section 3, the LCL-type grid-connected fuel cell inverter is modeled and analyzed. In section 4, the suggested current dual feedback control method is explained. A case study by the suggested method is investigated and compared with other methods. The system stability and sensitivity analysis are carried out in section 5. The simulation results and the conclusion are in sections 6 and 7, respectively.

2. CONSTRUCTION AND OPERATION OF THE FUEL CELL

2.1. Fuel Cell Construction

The fuel cell is a device that converts chemical energy into electrical energy. The inherent trend of hydrogen and oxygen is combination and water production. In fuel cells, this trend is utilized for electrical energy generation. As shown in Fig. 1, the fuel cell is constructed from the electrolyte and two electric poles as anode and cathode. The electrolyte has an important role in the fuel cell. In the fuel cell, ione displacement is conducted by necessary selectivity, and the two reaction factors are separated. Therefore, two half-reactions take place in the electrodes. It leads to generate electricity. In addition to it, each fuel cell has a catalyst. The electrolyte displaces the ions between electrodes while the catalyst increases the electrode reaction rates.

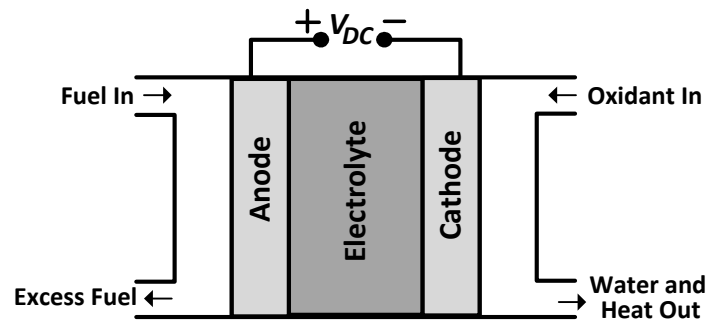


Fig. 1. Fuel cell construction.

2.2. Fuel Cell Operation

In the fuel cell, the anode and the cathode are continually fed by hydrogen and air oxygen, respectively. At the anode, the hydrogen molecule converts into two protons and two electrons. The electrolyte layer between the anode and the cathode permits only protons to transfer to the cathode. The electrolyte layer does not permit to transfer negative ions and acts as an insulator. Therefore, to reach the cathode, the electrons transfer the external circuit and produce the electrical current. At the cathode, recombination of the positive and negative ions and oxygen is conducted, and pure water is yielded [5].

The occurred chemical reactions in the fuel cell are given below.

1. The anode reaction



2. The cathode reaction



3. The total reaction



2.3. Fuel Cell Connection to the Grid

The grid-connected fuel cell with an LCL filter is shown in Fig. 2. Fuel cells produce DC voltage at their terminals, and to increase produced voltage level, DC-DC converters are often utilized [10]. Since the grids are AC, DC-AC converters are employed to transfer power from the fuel cells to the grids. Due to the switching process, voltage source inverters produce some distortions, which cause remarkable problems in the grid power quality. LCL filter utilized as an interface between the inverter and the grid is a solution for decreasing the distortions. LCL filter has zero impedance at the resonance frequency. This fact causes inverter instability. Toward stability, the resonance should be damped.

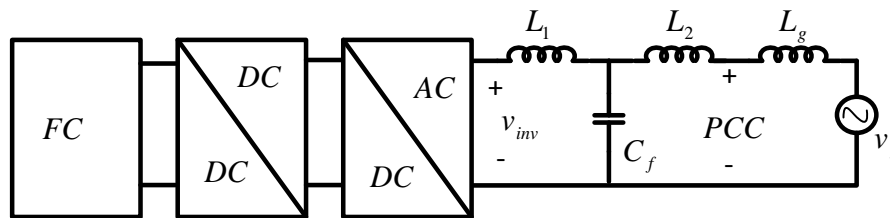


Fig. 2. Structure of the grid-connected fuel cell with LCL filter.

3. THE GRID-CONNECTED FUEL CELL WITH LCL FILTER

3.1. Model Description

The inverter side and the grid side inductance currents control strategy is proposed to inject high-quality current and improve the stability of the inverter-based grid-connected fuel cell with an LCL filter (GCFCI-LCL). The schematic of GCFCI-LCL and its control structure are illustrated in Fig. 3. In this figure, L_1 , C_f , and L_2 are inverter side inductance, capacitor, and grid side inductance of the LCL filter, respectively. Also, i_1 , i_2 , and i_c are inverter side and grid side currents and capacitor current, respectively. Moreover, v_{inv} , v_g , and v_{PCC} are inverter side voltage, grid voltage, and point of the common coupling voltage, respectively. The total grid impedance at PCC is modeled by an inductance and a resistance. By Phase Locked Loop (PLL), the reference current and the grid voltage become synchronous. Yielded signal from the reference current and PLL output signal is compared with the current of L_2 , and then the error signal feeds the current regulator G_i . The suggested control strategy is based on the feedback of two currents, the currents of the inverter side inductance and the grid side inductance. So, the output signal of the current regulator G_i is compared with the inverter side current, and the switching reference signal is generated. Unipolar PWM is utilized for switching the inverter. Hence, the effective frequency of the harmonics appears at $2f_s$.

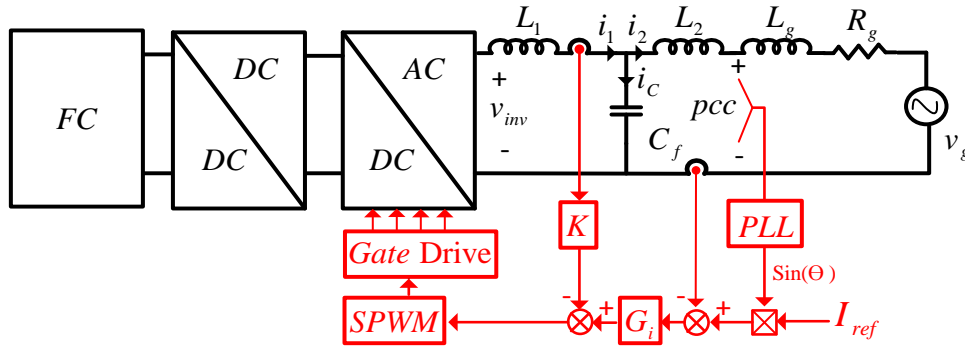


Fig. 3. Power circuit and the suggested control scheme for the grid-connected fuel cell inverter.

3.2. Filter Design

The inverter side inductance current ripple is determined by the inverter output voltage (v_{inv}) and filter capacitor voltage (v_c). This inductance faces high-frequency current ripple. The core loss depends on the circuit operation frequency highly. Therefore, the core loss in the inverter side inductance is high. The filter capacitor damps the high-frequency ripples and allows the grid currents with limited frequency to pass. The grid side inductance (L_2) attenuates the grid side harmonics. In the inductances sizing, some constraints should be considered. If L_1 is chosen large, the cost and the loss will increase. If L_2 is chosen large, the high-frequency harmonics will be better attenuated. On the other hand, the summation of L_1 and L_2 should not be too large. This condition leads to a voltage drop at the fundamental frequency. The inductance values are calculated as:

$$L_1 + L_2 \leq \frac{v_{inv} - v_g}{2\pi f_0 i_g} \tag{4}$$

where f_0 is output frequency, and i_g is grid current.

Large capacitor choices can increase reactive power and change the power factor. The capacitor's reactive power constrain is as:

$$2\% \times S_n \leq Q_C \leq 5\% \times S_n \tag{5}$$

$$C = \frac{Q_C}{\omega_0 V^2} \Rightarrow \begin{cases} C \leq \frac{0.05 \times S_n}{\omega_0 V_{ph}^2} \\ C \geq \frac{.02 \times S_n}{\omega_0 V_{ph}^2} \end{cases} \tag{6}$$

where ω_0 is output angular frequency, and V_{ph} is output effective phase voltage [26].

3.3. Analysis and Control of the LCL-Type Grid-Connected Fuel Cell Inverter

In the control scheme of the LCL-type grid-connected fuel cell inverter, the inverter transfer function is $K_{PWM} = v_{in} / v_{tri}$, where v_{tri} and v_{inv} are triangle carrier signal amplitude and output voltage of H-bridge, respectively. The suggested control strategy is based on the feedback of two currents, the current of the inverter side inductance and the grid side inductance. The control scheme includes two control loops. The external loop deals with the grid side current feedback. The internal loop deals with the inverter voltage control, which uses the inverter side current with constant coefficient K as virtual impedance. The scheme is demonstrated in Fig. 4. In the external loop, the G_i current regulator is employed to regulate the grid side current. It is a PI controller as:

$$G_i = K_p + \frac{K_i}{S} \tag{7}$$

According to Fig. 4, the transfer function of the LCL filter can be explored as:

$$G_{LCL} = \frac{1}{L_1 L_2 C S^3 + (L_1 + L_2) S} \tag{8}$$

and the LCL filter resonance frequency is:

$$f_{LCL} = \frac{1}{2\pi} \sqrt{\frac{L_1 + L_2}{L_1 L_2 C}} \tag{9}$$

In digital control, there are computational and PWM delays. Computational delay deals with sampling time and PWM reference updating. Zero Order Hold (ZOH) causes PWM delay. ZOH fixes the PWM references after each update. This delay is defined as:

$$G_D(S) = \frac{1}{T_s} e^{-\lambda s T_s} \cdot \frac{1 - e^{-s T_s}}{S} \approx e^{-1.5 s T_s}; (0 \leq \lambda \leq 1) \tag{10}$$

where $e^{-s T_s}$ is the time delay of a sampling period, $1/T_s$ is the sampling frequency, and $(1 - e^{-s T_s})/S$ is Zero Order Hold (ZOH).

The control scheme of LCL-type grid-connected fuel cell inverter under the conventional as well as the proposed strategy by considering time delay is shown in Fig. 4. The conventional strategy shown in Fig. 4(a) is based on the capacitor current active damping method, which utilizes the feedback of the capacitor current and the network side inductor current to dampen the resonance of the LCL filter. In the proposed control strategy shown in Fig. 4(b), inverter side and grid side inductor currents feedback are used to dampen the LCL filter resonance. There are two completely separate loops in the proposed control strategy, and the K_{PWM} coefficient is added to the transfer function of the conventional strategy, which results in better resonance damping and stability capability.

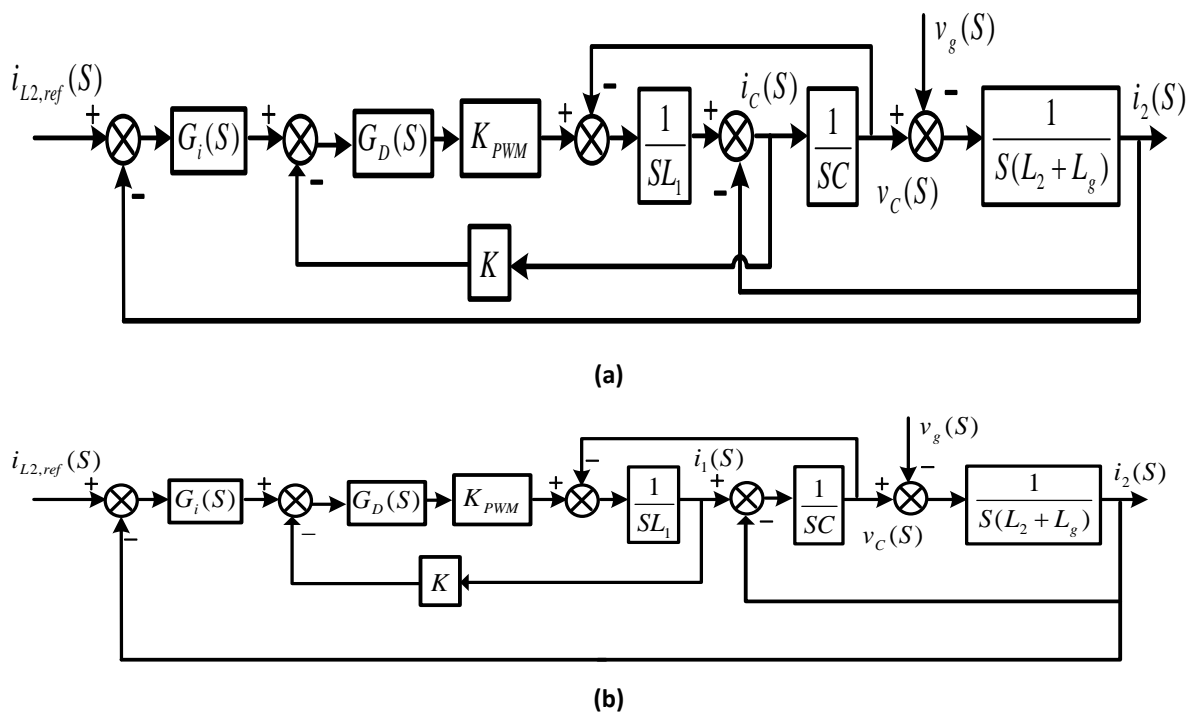


Fig. 4. Block diagram of the grid-connected fuel cell inverter under: a) conventional control scheme; b) the suggested control scheme.

As shown in Fig. 4, the control system output is the injected current to the grid (i_g). The control system inputs are the reference injected current to the grid ($i_{L2,ref}$) and the grid voltage (v_g). By Mason's gain formula, the open-loop transfer function of the system (i_{g-ol}) in the presence of the grid side current regulator G_i can be yielded as [27]:

$$i_{g-ol} = \frac{K_{P_{PWM}} G_i(s)}{L_1(L_2 + L_g)Cs^3 + C(L_2 + L_g)KK_{P_{PWM}}s^2 + (L_1 + L_2 + L_g)s + KK_{P_{PWM}}} \times i_{L2,ref} - \frac{s^2 L_1 C + sCK_{P_{PWM}}K + 1}{L_1(L_2 + L_g)Cs^3 + C(L_2 + L_g)KK_{P_{PWM}}s^2 + (L_1 + L_2 + L_g)s + KK_{P_{PWM}} + K_{P_{PWM}}G_i} \times v_g \quad (11)$$

4. SYSTEMATIC DESIGN OF THE SUGGESTED CONTROL SYSTEM PARAMETERS

In the suggested control strategy, K is the feedback coefficient of the inverter side inductance current. K_p and K_i are the PI controller parameters in the current regulator (G_i). These parameters affect GCFCI-LCL operation indexes, such as resonance damping, stability margin, and grid connection properties. The desirable performance design process of the parameters is as follows:

1. Stability margin of the parameters.
2. Determining K based on damping LCL filter resonance by the inverter side inductance current feedback.
3. Proposing a simple low-frequency model.
4. Design of the PI controller parameters by considering grid connection mandatories and the system stability.

4.1. Stability Margin of the Parameters by Considering Time Delay by Routh-Hurwitz Stability Criterion

By Mason's gain formula, the closed-loop transfer function (i_{g-cl}) of the suggested control system for GCFCI-LCL, which is based on double feedback, can be resulted as:

$$i_{g-cl} = \frac{K_{P_{PWM}} G_i(s)}{L_1(L_2 + L_g)Cs^3 + C(L_2 + L_g)KK_{P_{PWM}}s^2 + (L_1 + L_2 + L_g)s + KK_{P_{PWM}} + K_{P_{PWM}}G_i} \times i_{L2,ref} - \frac{s^2 L_1 C + sCK_{P_{PWM}}K + 1}{L_1(L_2 + L_g)Cs^3 + C(L_2 + L_g)KK_{P_{PWM}}s^2 + (L_1 + L_2 + L_g)s + KK_{P_{PWM}} + K_{P_{PWM}}G_i} \times v_g \quad (12)$$

By Taylor series, time delay G_D can be written as:

$$G_D(s) = \frac{1}{1 + 1.5T_s s} \quad (13)$$

By Eqs. (7), (12), and (13), the characteristic equation of the closed-loop system $G_{CL}(s)$ can be yielded as Eq. (14).

$$G_{CL}(s) = 1.5L_1(L_2 + L_g)CT_s s^5 + L_1(L_2 + L_g)Cs^4 + [(L_2 + L_g)CKK_{P_{PWM}} + 1.5(L_1 + L_2 + L_g)T_s]s^3 + (L_1 + L_2 + L_g)s^2 + (K + K_p)K_{P_{PWM}}s + K_i K_{P_{PWM}} \quad (14)$$

According to the Routh-Hurwitz stability criterion, the poles of the closed-loop system must be placed in the left half-plane in the stable systems. Furthermore, elements of the first

column of the Routh table and characteristic equation roots must be in the same sign or positive sign. To ensure the stability of the GCFCI-LCL system, the range of the K , K_p , and K_i is calculated as Eq. (15), where R_{S1} can be yielded based on the Routh-Hurwitz stability criterion as Eq. (16).

$$\begin{cases} K > \frac{L_1}{L_2 + L_g} (K_p - K_i) \\ K + K_p > K_i > \frac{L_1}{L_2 + L_g} (K_p - K) \\ \frac{L_2 + L_g}{L_1} K + K_i > K_p > K_i - K \\ R_{S1} > 0 \end{cases} \quad (15)$$

$$R_{S1} = \frac{(L_2 + L_g)(K^2 K_{PWM} + KK_p K_{PWM} - CKK_{PWM}^2 K_i) - L_1(KK_p K_{PWM} + K_p^2 K_{PWM})}{(L_2 + L_g)K - L_1 K_p} \quad (16)$$

By increasing the grid inductance (L_g), the total harmonic of the system increases. Thereby, to ensure the stability of the GCFCI-LCL system, the range of the K , K_p , and K_i must be increased according to Eq. (16).

4.2. The Inverter Side Inductance Current Feedback and Simple Low-Frequency Model

The inverter side current feedback and simple low-frequency model of the GCFCI-LCL system are demonstrated in Fig. 5.

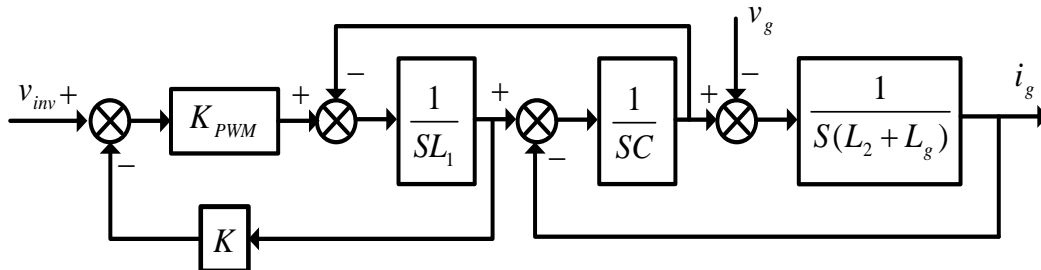


Fig. 5. Block diagram of the inverter side current feedback control.

As shown in Fig. 5, by Mason's gain formula, the characteristic equation of the open-loop transfer function can be expressed as:

$$D_0(s) = as^3 + bs^2 + cs + d \quad (17)$$

where $a=L_1(L_g+L_2)C$, $b=C.K.(L_g+L_2) K_{PWM}$, $c=L_g+L_1+L_2$ and $d= K.K_{PWM}$. Comparing Eqs. (8) and (17), the added damping components are $CL_2KK_{PWM}S^2$ and KK_{PWM} . The third-order system stability condition is that all coefficients be existent and have the same sign, and also, $bc>ad$. Based on the Cardano method, if K is bigger than zero, Δ will be bigger than zero. Thus,

$$\begin{aligned} \Delta &= (ba - 9ad)^2 - 4(b^2 - 3ac)(c^2 - 3bd) \\ &= 3L_2^6 \left[\begin{array}{l} e^2 K^2 K_{PWM}^2 (27y^3 + 26y^2 - 2y - 1) + \\ 4(1+y)^3 ye + 4e^3 K^4 K_{PWM}^4 \end{array} \right] > 0 \end{aligned} \quad (18)$$

Eq. (18) has a real root and two complex conjugate roots. The characteristic equation of the open-loop system transfer function can be written as:

$$D_0(s) = (mS + n)(S^2 + \xi\omega_r S + \omega_r^2) = 0 \quad (19)$$

where $-n/m$, ξ , and ω_r are real root, damping ratio, and resonance frequency, respectively.

$$\begin{cases} \zeta = \frac{-b + \frac{1}{2}(\sqrt[3]{Y_1} + \sqrt[3]{Y_2})}{3a\omega_r} \\ \omega_r = \frac{1}{3a} \sqrt{\left[-b + \frac{1}{2}(\sqrt[3]{Y_1} + \sqrt[3]{Y_2})\right]^2 + \frac{3}{4}(\sqrt[3]{Y_1} + \sqrt[3]{Y_2})^2} \\ n = \frac{-b - \frac{1}{2}(\sqrt[3]{Y_1} + \sqrt[3]{Y_2})}{3a\omega_r} \\ m = \frac{-b - \frac{1}{2}(\sqrt[3]{Y_1} + \sqrt[3]{Y_2})}{3a\omega_r} \end{cases} \quad (20)$$

$$\begin{cases} e = C / (L_2 + L_g), \quad y = L_1 / (L_2 + L_g) \\ Y_{1,2} = e^2 L_2^6 K K_{PWM} \left[K^2 K_{PWM}^2 - 3ey(1+y) \right] + \\ \frac{3}{2} ey L_2^3 \left[e L_2^3 K K_{PWM} (8y-1) \pm \sqrt{\Delta} \right] \end{cases} \quad (21)$$

Resonance frequency in the GCFCI-LCL system shows an important role in harmonic damping. If the resonance frequency is between $10f_n$ and $1/3f_s$, better current harmonics damping and dynamic response can be attained [28]. Based on Eq. (20), the feedback coefficient of the inverter side current (K), damping ratio (ξ), and resonance frequency (ω_r) have a significant role in the system stability. K must be chosen in its stability range described by Eq. (15). The design trend of the ξ , K , and ω_r is summarized in the flowchart as shown in Fig. 6. First, the resonance frequency of the GCFCI-LCL can be specified by switching frequency. Then, the range of K is resulted by Eq. (20). If K is in a stable range, the desirable damping ratio (ξ) can be yielded in the next step. Otherwise, K and ω_r values must be changed until they place in a stable range according to Eq. (15). Then, the desired damping ratio (ξ) is determined. Finally, K and ω_r values are calculated.

For the GCFCI-LCL with inverter side current feedback control, shown in Fig. 5, the bode diagram for variation of K is depicted in Fig. 7. As shown in the diagram, when $K = 0$, active damping has no role in resonance damping, and the system has a zero impedance at the resonance frequency. By increasing k , the diagram amplitude decreases at the resonance point. Therefore, the resonance can be damped by active damping effectively. Then, the system becomes stable. In the active damping, the inverter side current feedback damps LCL filter resonance. If $K = 0$, the system frequency and the resonance frequency will be equal ($\omega = \omega_r$). In this condition, the phase diagram does not depend on ξ , and its value is -90 degrees. By increasing K , the damping ratio increases. The damping ratio determines resonance amplitude. Therefore, the system cutoff frequency (ω_c) is smaller than the resonance frequency (ω_r), and the resonance is damped. To simplify the systematic design trend of the parameters, the simplified low-frequency transfer function from i_2 to v_{inv} is proposed as:

$$\frac{i_2}{v_{inv}} = \frac{1}{K} \quad (22)$$

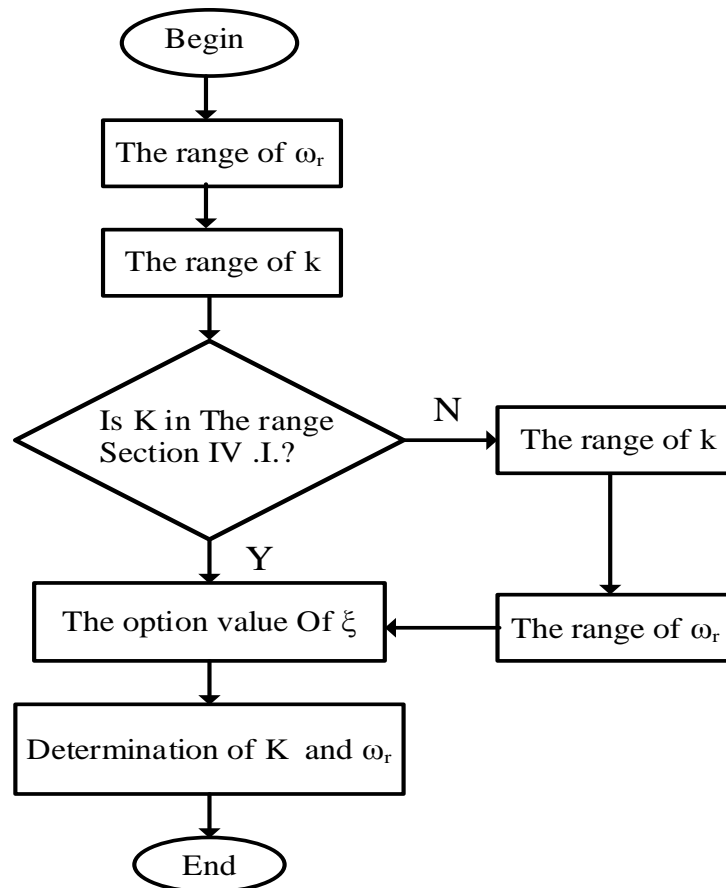


Fig. 6. K design trend summarization in the inverter side current feedback control.

The phase-frequency diagram starts from zero according to Eq. (22). The magnitude-frequency diagram becomes parallel with the frequency axis. In low frequencies around the fundamental frequency, these diagrams are matched with bode diagrams, which are shown in Fig. 7.

4.3. Design of the Current Regulator Parameters

Proportional and integral gains of the current regulator G_i highly effect on stability and reliability of the GCFCI-LCL. In this section, PI controller parameters are determined based on stability margin and dynamic response.

The resonance frequency of the GCFCI-LCL is calculated by Eq. (20) and based on Fig. 6. In the bode diagram of the system open-loop transfer function, the cross point between the phase diagram and -180 degree is the LCL filter resonance frequency. Closely, the phase margin deals with the transient behavior of the closed-loop system. A smaller overshoot can be obtained by increasing the phase margin. In Gain Margin (GM) design, the GCFCI-LCL system with the inverter side current feedback is considered. The GM should be as follows.

$$-20 \log \left| \left(K_p + \frac{K_i}{s} \right) \cdot \frac{K_{PWM}}{L_1(L_2 + L_g)Cs^3 + CL_2KK_{PWM}s^2 + (L_1 + L_2 + L_g)s + KK_{PWM}} \right|_{s=j\omega_r} \geq GM \quad (23)$$

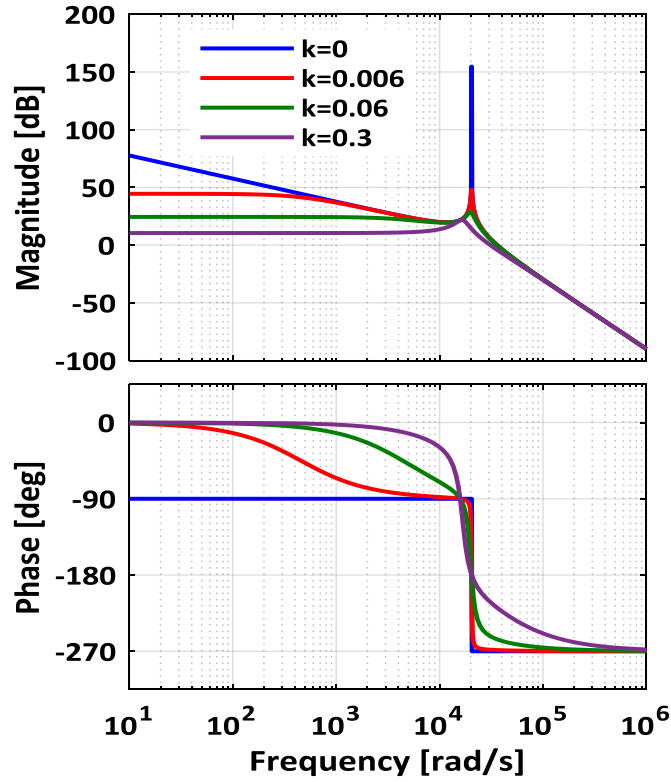


Fig. 7. Bode diagram for the inverter side current feedback by variation of K .

By increasing the grid impedance (L_g), the phase margin decreases. Therefore, to increase the system stability, K_p range should be increased. In the ideal grid, the K_p range is:

$$K_p \geq \frac{\left| L_1 L_2 C s^3 + C L_2 K K_{PWM} s^2 + (L_1 + L_2) s + K K_{PWM} \right|_{s=j2\pi f_{LCL}}}{K_{PWM} \times 10^{20}} \quad (24)$$

According to Eq.(24), if C or L_1 values increase, then K_p range will decrease. The phase cross frequency (ω_c) in the GCFCI-LCL system is significantly smaller than LCL the filter resonance frequency. Therefore, the open-loop transfer function or low-frequency transfer function with a PI controller is as:

$$G_{OP} = \left(K_p + \frac{K_i}{s} \right) \cdot \frac{1}{K} \quad (25)$$

The system Phase Margin (PM) can be described as:

$$180^\circ + \angle \frac{(K_p s + K_i)}{sK} \geq PM \quad (26)$$

Generally, in a control system with desirable stability PM value should be more than 45 degrees. By considering the cross-frequency of phase (ω_c) in Eq. (27), the range of the K_p and K_i can be yielded by Eqs. (28) and (29).

$$\omega_c \propto \frac{K_{I2}}{\sqrt{K^2 - K_p^2}} \leq 10 f_n \times 2\pi \quad (27)$$

$$0 \leq K_p \leq K \quad (28)$$

$$K_i \leq 10 f_0 \times 2\pi \times \sqrt{K^2 - K_p^2} \quad (29)$$

4.4. Comparing the Suggested and the Traditional Control Strategies

In controller design for the GCFCI-LCL system, the grid impedance (L_g) is assumed to be a part of the grid inductance. The system is analyzed by varying the grid impedance. To ensure desirable dynamic response and stability margin, $PM \geq 45^\circ$ and $GM \geq 3\text{dB}$ are adopted. Bode diagrams of the GCFCI-LCL system for the suggested control strategy and the traditional control scheme, which is based on capacitor current and the grid side inductance current feedback, are illustrated in Fig. 8. For an ideal grid ($L_g = 0$), the phase margin and the gain margin in the suggested control strategy are 105.4° and 4.16 dB, respectively. Moreover, in the traditional control strategy, they are 23° and 3.76 dB. Increasing the grid impedance ($L_g = 0.8$ mH), the phase margin and the gain margin in the suggested control strategy are 90.2° and 10.7 dB, respectively. Moreover, in the traditional control strategy, they are 32.1° and 14.1 dB. In other case ($L_g = 4.8$ mH), the phase margin and the gain margin in the suggested control strategy are 57.2° and 22.8 dB, respectively. Furthermore, in the traditional control strategy, they are 19.5° and 23.7 dB. In the suggested control strategy, by changing the grid impedance, the system open-loop transfer function magnitude at the fundamental frequency ($\omega_n = 100\pi$) is fixed and 13 dB. However, by changing the grid impedance in the traditional control strategy, the system open-loop transfer function magnitude at the fundamental frequency ($\omega_n = 100\pi$) is variable. From a damping point of view, the system's dynamic response and the stability margin are better than traditional control.

Bode diagrams of the weak grid-connected system by traditional active damping strategy for different values of the grid inductance, such as $L_g=0$, $L_g=0.8$ mH, and $L_g=4.8$ mH, are shown in Fig. 8. By the traditional active damping approach, based on the grid and capacitor currents feedback, the magnitude of the open-loop transfer function at the fundamental frequency varies from 36.9 dB to 21.6 dB. GM and PM values are changed from 3.76 dB to 23.7 dB and 23° to 19.5° , respectively. Therefore, by increasing L_g in the traditional active damping approach, the system stability requirements do not satisfy. Compared with the traditional active damping approach, the suggested strategy is more stable and shows better resonance damping characteristics for the low-frequency range. Thus, by changing LCL filter parameters, especially the grid impedance L_g , the system performance is desirable for the weak grid.

5. SYSTEM STABILITY AND SENSITIVITY ANALYSIS

A design example for the GCFCI-LCL system by the suggested control strategy is investigated in this section. Also, system stability is investigated, and sensitivity analysis is conducted. The main parameters of the GCFCI-LCL system are presented in Table 1. The resonance frequency is between $10f_0$ and $0.5f_s$, where f_0 is the fundamental frequency, and f_s is the switching frequency.

According to the characteristic equation of the closed-loop system in Eq. (14), K , K_p , and K_i are positive. Their ranges based on the Routh-Hurwitz stability criterion are as:

$$K + K_p > K_i > K_p - K \quad (30)$$

$$(K + K_p) - K_i - \frac{CKK_{PWM}K_i}{K - (K_p - K_i)} > 0 \quad (31)$$

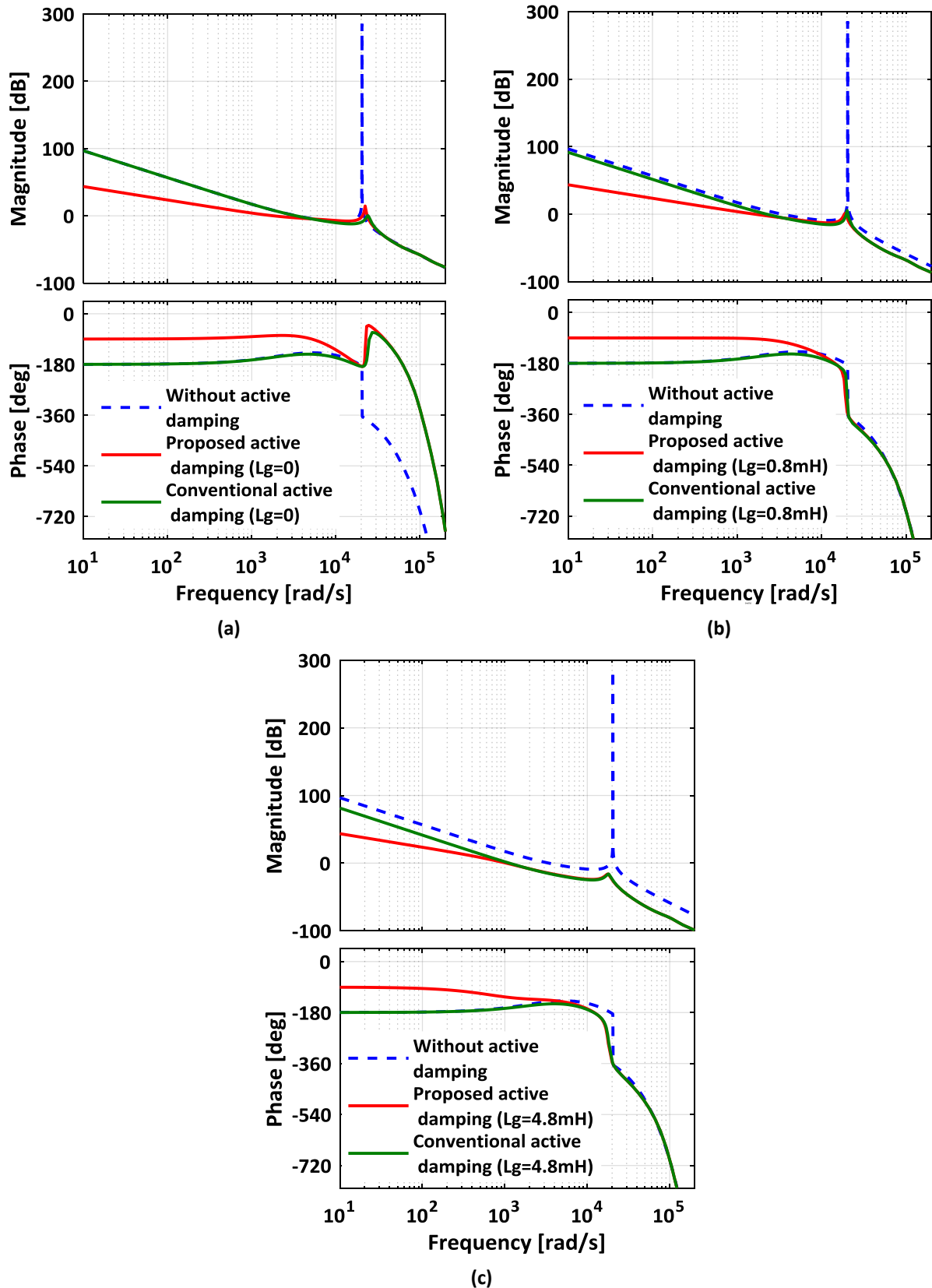


Fig. 8. Bode diagram for the GCFCI-LCL system under the traditional and the suggested control schemes: a) $L_g = 0$ mH; b) $L_g = 0.8$ mH; c) $L_g = 4.8$ mH.

The current controller parameter ranges are illustrated in Fig. 9. To achieve LCL filter damping, K must be determined. As Eq. (15), K and ω_r are calculated 0.06 and 20500 rad/s,

respectively. To supply the system requirements, $GM > 3 \text{ dB}$ and $PM > 45^\circ$ are chosen at nominal power (P_n). K_p and K_i are calculated by Eqs. (23) and (28) to (31). By considering a variation of the $L_1(\pm 20\%)$, $L_2(\pm 20\%)$, and $C(\pm 20\%)$, the K_p range varies between $[0.025, 0.057]$ and $[0.035, 0.057]$. Then, the point of A in Fig. 9 and the current controller is adjusted ($K_p = 0.04$, $K_i = 90$) to increase the stability margin. The open-loop transfer function magnitude at the fundamental frequency is 13 dB. PM and GM are 105.4° and 4.16 dB, respectively. Therefore, stability is warranted. However, as shown in Fig. 9, point B ($K_p = 0.027$, $K_i = 90$) is out of the region and stability is warranted, where PM and GM are 95.6° and 8.3 dB, respectively. Similarly, point C ($K_p = 0.05$, $K_i = 150$) is out of the region, where PM and GM are 94.5° and 2.83 dB, respectively. The system stability requirement does not satisfy. Therefore, based on Eqs. (26) to (29), the shaded area warrants the system's stable operation and supplies the grid connect system requirements.

Table 1. Main parameters of the GCFCI-LCL system.

Parameter	Value
Inverter side inductor (L_1)	0.6 mH
Inverter side inductor (L_2)	0.4 mH
Filter capacitor (C_i)	10 μF
Mains RMS voltage (V_g)	220 V
Fundamental frequency (f_o)	50 Hz
Switching frequency (f_s)	10 KHz
Feedback coefficient of the inverter side current (K)	0.06
Peak voltage of inverter output (V_{inv})	360 V
Peak amplitude of carrier signal (V_{tri})	4.57

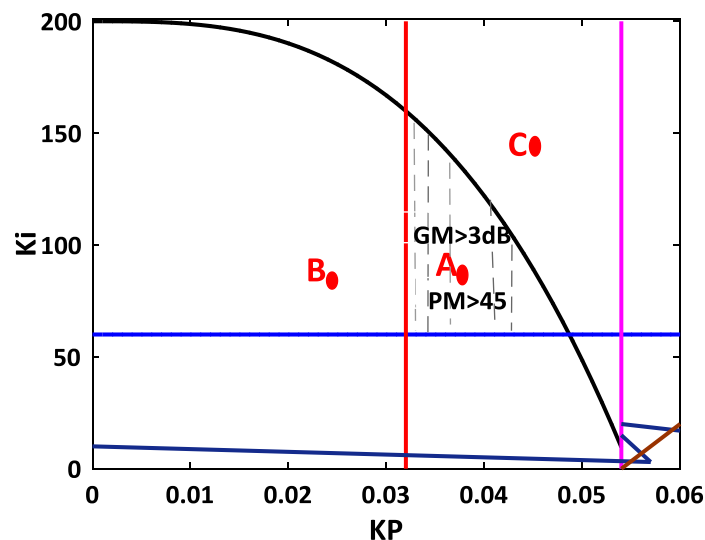


Fig. 9. Parameter variation in the PI controller.

The pole-zero plot for the open-loop system with current regulator G_i by increasing K is depicted in Fig. 10. The grid impedance is $L_g = 0.8 \text{ mH}$. By increasing K , the zeros and the poles are in the unit circle, and the system is stable.

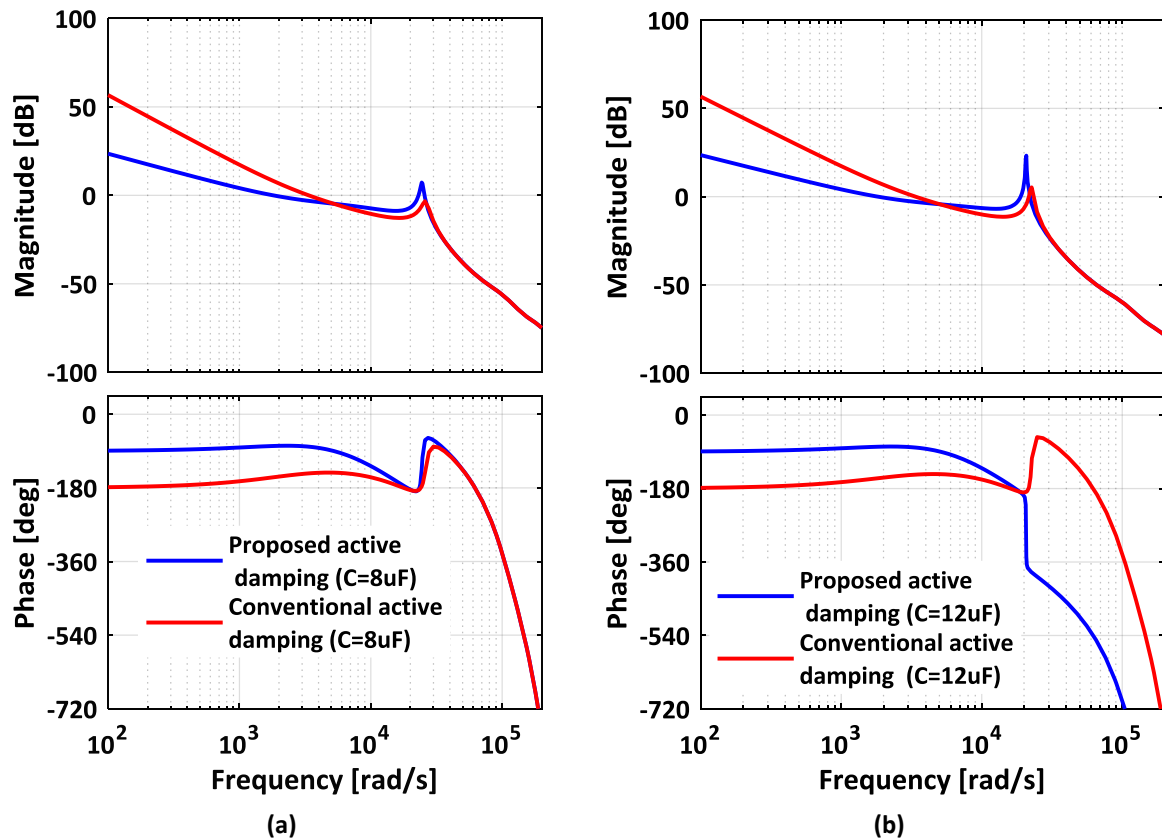


Fig. 11. Bode diagrams of the GCFCI-LCL system by varying LCL filter capacitance: a) $C_f = 8 \mu\text{F}$; b) $C_f = 12 \mu\text{F}$.

The designed value of the inverter side inductor of the LCL filter is 0.6 mH, and $\pm 20\%$ change is considered from 0.48 mH to 0.72 mH to investigate the system sensitivity. The bode diagram of the studied system for both suggested and conventional control schemes considering $L_1 = 0.48$ mH is shown in Fig. 12(a), and for $L_1 = 0.72$ mH is presented in Fig. 12(b). When $L_1 = 0.48$ mH, the magnitude of the open-loop transfer function at the fundamental frequency under the suggested control scheme is fixed at 13.6 dB, and the GM and PM values are 5.43 dB and 105.9° , respectively. All of the requirements are satisfied by the suggested control scheme. In contrast, the magnitude of the open-loop transfer function at the fundamental frequency under the conventional control scheme is fixed at 38 dB, and the GM and PM values are 11.8 dB and 35° , respectively. Although the system is stable, the PM is lower than 45° , and the requirements are not satisfied. Considering $L_1 = 0.72$ mH, the magnitude of the open-loop transfer function at the fundamental frequency under the suggested control scheme is 13.6 dB, and the GM and PM values are 4.49 dB and 99.8° , respectively. Therefore, all of the requirements are satisfied by the suggested control scheme. Reciprocally, the magnitude of the open-loop transfer function at the fundamental frequency under the conventional control scheme is 35.9 dB, and the GM and PM values are 11.6 dB and 34° , respectively. Although the system is stable, the PM is lower than 45° , and the requirements at $L_1 = 0.72$ mH are not satisfied. Comparing the results of Figs. 12(a) and 12(b) depicts that by varying L_1 , the suggested control strategy satisfies the requirements, while the requirements are not provided in the traditional control strategy.

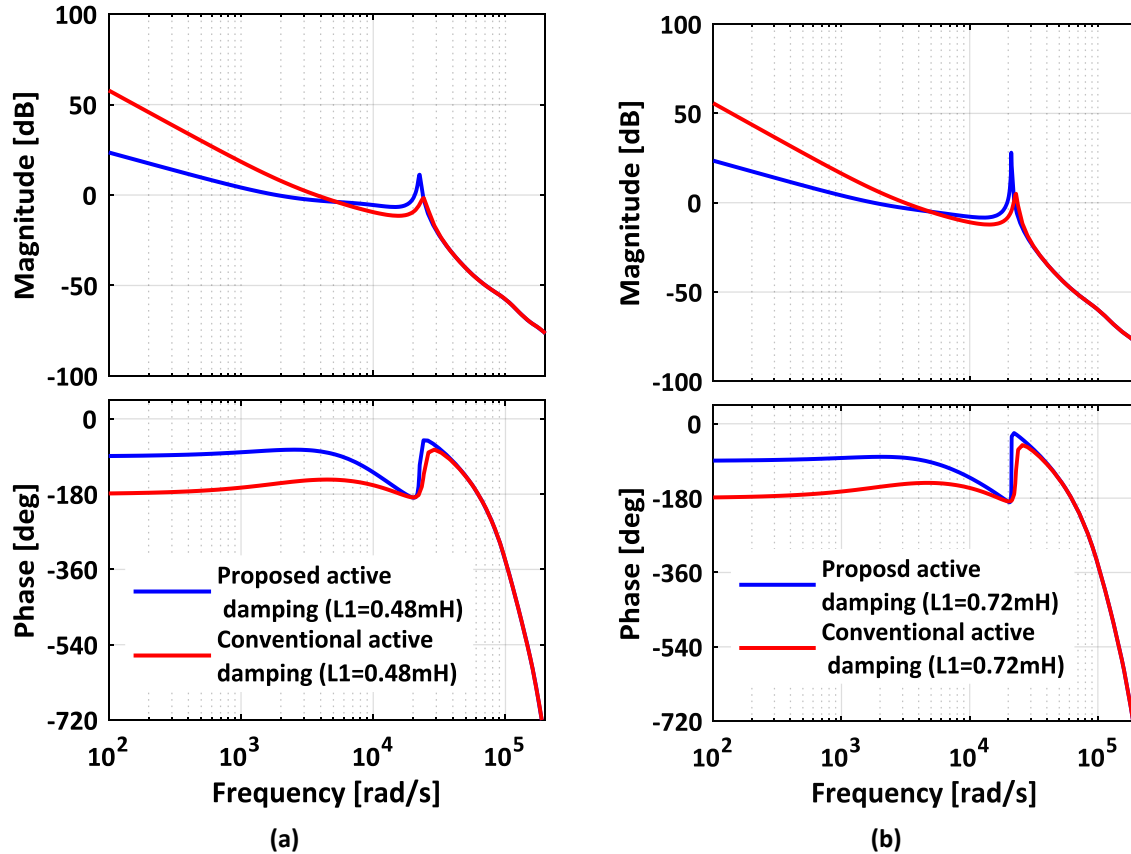


Fig. 12. Bode diagrams of the GCFCI-LCL system by varying LCL filter's inverter side inductance: a) $L_1 = 0.48$ mH; b) $L_1 = 0.72$ mH.

The designed value of the grid side inductor of the LCL filter is 0.4 mH, and $\pm 20\%$ change is considered from 0.32 mH to 0.48 mH to investigate the system sensitivity. The bode diagram of the studied system for both suggested and conventional control schemes considering $L_2 = 0.32$ mH is shown in Fig. 13(a), and for $L_2 = 0.48$ mH is presented in Fig. 13(b). When $L_2 = 0.32$ mH, the magnitude of the open-loop transfer function at the fundamental frequency under the suggested control scheme is fixed at 13.6 dB, and the GM and PM values are 6.26 dB and 102.2° , respectively. All of the requirements are satisfied by the suggested control scheme. In contrast, the magnitude of the open-loop transfer function at the fundamental frequency under the conventional control scheme is fixed at 36.9 dB, and the GM and PM values are 5.47 dB and 35.7° , respectively. Although the system is stable, the PM is lower than 45° , and the requirements are not satisfied. Considering $L_2 = 0.48$ mH, the magnitude of the open-loop transfer function at the fundamental frequency under the suggested control scheme is 13.6 dB, and the GM and PM values are 6.13 dB and 100.6° , respectively. Therefore, all of the requirements are satisfied by the suggested control scheme. Reciprocally, the magnitude of the open-loop transfer function at the fundamental frequency under the conventional control scheme is 36.2 dB, and the GM and PM values are 12 dB and 34° , respectively. Although the system is stable, the PM is lower than 45° , and the requirements at $L_2 = 0.48$ mH are not satisfied. Comparing the results of Figs. 13(a) and 13(b) describes that by varying L_2 , the suggested control scheme satisfies the requirements, while the requirements are not provided in the conventional control scheme.

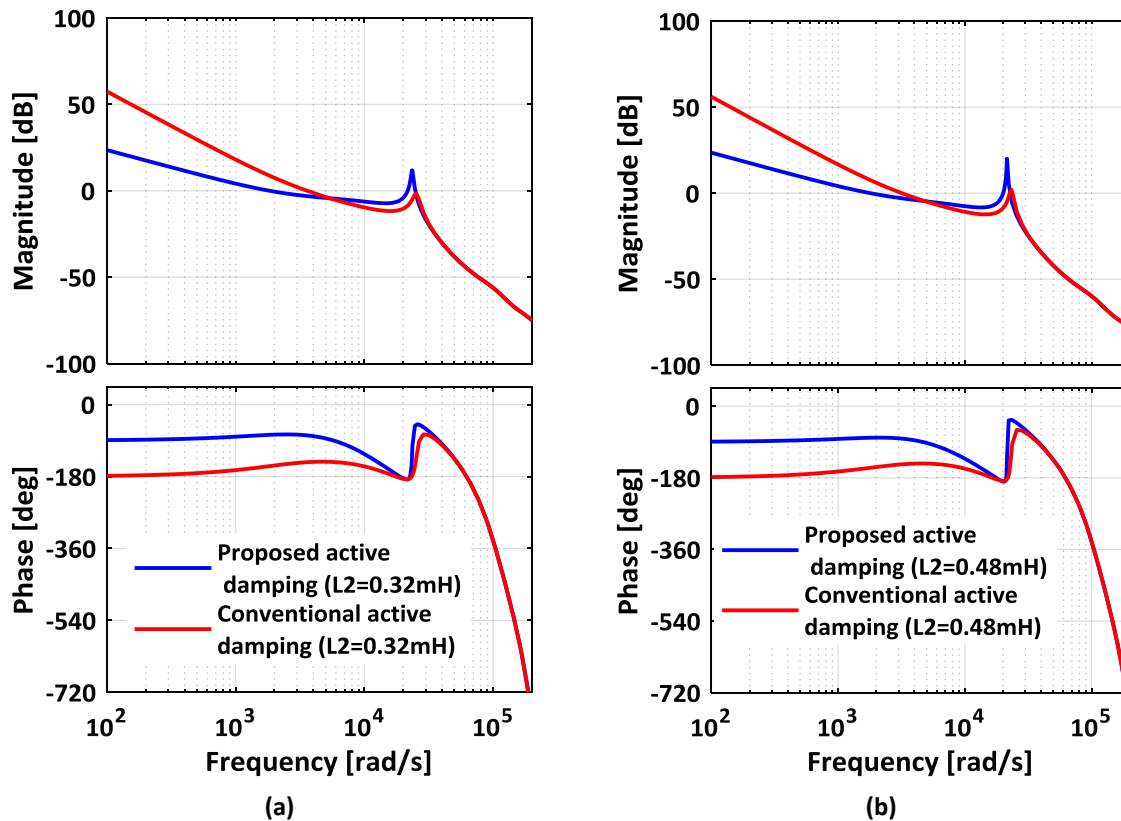


Fig. 13. Bode diagrams of the GCFCI-LCL system by varying LCL filter's grid side inductance: a) $L_2 = 0.32$ mH; b) $L_2 = 0.48$ mH.

6. SIMULATION RESULTS

6.1. Steady State Operation

The operation of GCFCI-LCL system at the steady state condition is investigated in this section. The voltage, current, and power of the fuel cell, which includes 65 series cells, are shown in Fig. 14. The total voltage of the series cells is 52.4 V, and the fuel cell supplies 113 A. The fuel cell produced power, which is yielded by multiplying voltage and current, is 6 kW. The delivered power into the grid is 5.75 kW. The voltage of the Point of Common Coupling (PCC) and the normalized injected current to the weak grid based on the suggested method are shown in Fig. 14(e). The PCC voltage (v_g) is stable and without harmonic distortions. The Total Harmonic Distortion (THD) of the grid injected current is 1.10%.

6.2. The System Stability by Varying K

For the ideal grid ($L_g = 0$), the coefficient K varies from 0.06 to zero. The simulation results of the suggested strategy are shown in Fig. 15. Before $t = 1$ s, the GCFCI-LCL system operates with the suggested control strategy at full load continuously. At $t = 1$ s, K changes suddenly from 0.06 to 0, and the grid current (i_2) increases rapidly. At $t = 1.3$ s, the injected current is more than the overload current. Then, the GCFCI-LCL system becomes unstable and disconnects from the grid. Therefore, the GCFCI-LCL system with the suggested active damping strategy operates continuously at $K = 0.06$. The grid current, the fuel cell current, the fuel cell generated power and the fuel cell open circuit voltage are presented in Fig. 15, respectively.

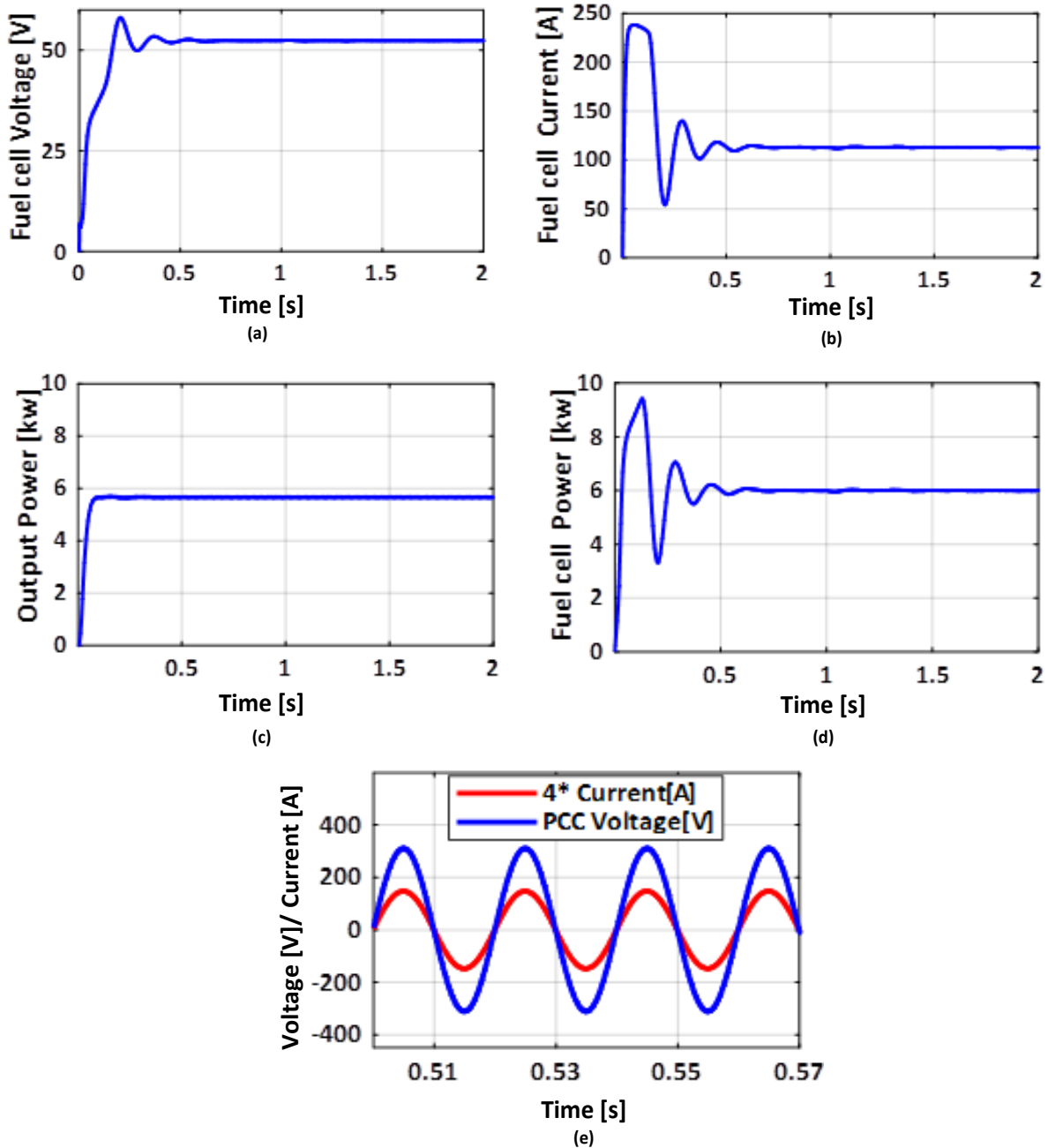


Fig. 14. The investigated fuel cell parameters: a) the output voltage; b) the output current; c) the fuel cell power; d) the delivered power; e) the PCC voltage and current.

6.3. The Fuel Flow Variation

Voltage-current characteristics of a fuel cell depends on the fuel flow rate. From $t = 1$ s to $t = 1.4$ s, it is assumed that the fuel flow is reduced by 20%. This condition is simulated. Voltage and current reduction are expected by reducing the flow. According to Figs. 16(a) and 16(b), the fuel cell voltage and current reduce as same as the flow reduction rate. These reductions cause to reduce in generated and delivered power by the fuel cell, as shown in Figs. 16(c) and 16(d). After an instantaneous voltage drop at $t = 1$ s, by the proper performance of the DC-DC converter, the DC link voltage comes back to 350 V again, as shown in Fig. 16(e).

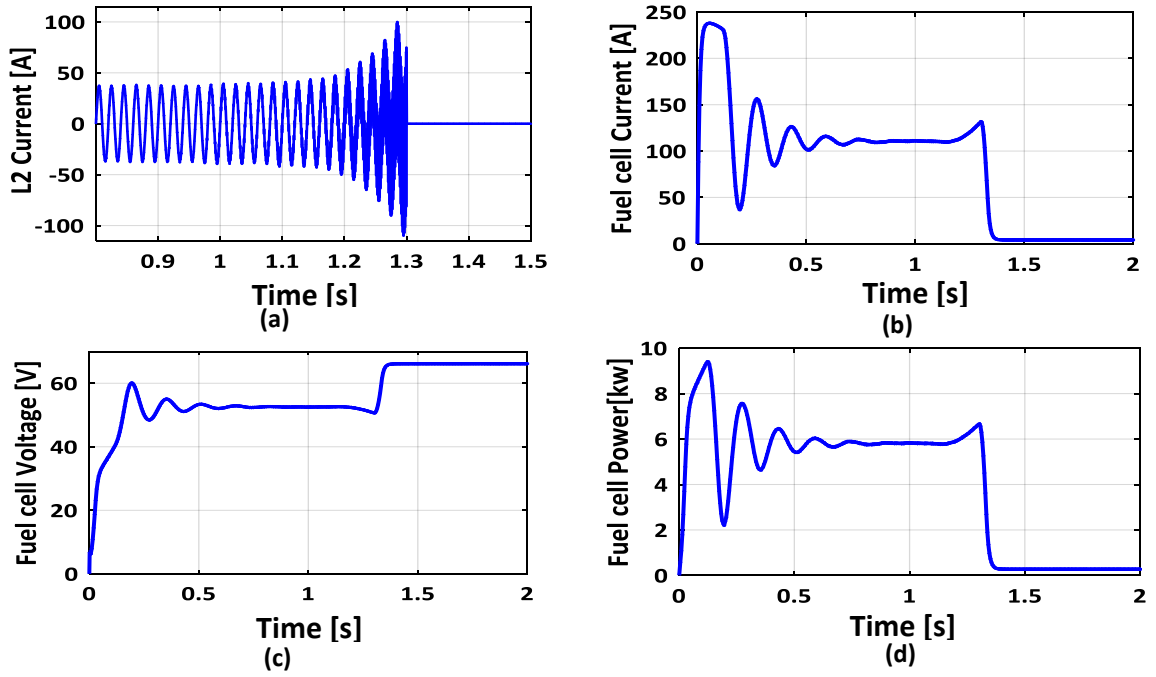


Fig. 15. The operation of the investigated system with a step change in K value: a) grid current; b) fuel cell current; c) fuel cell voltage; d) fuel cell power.

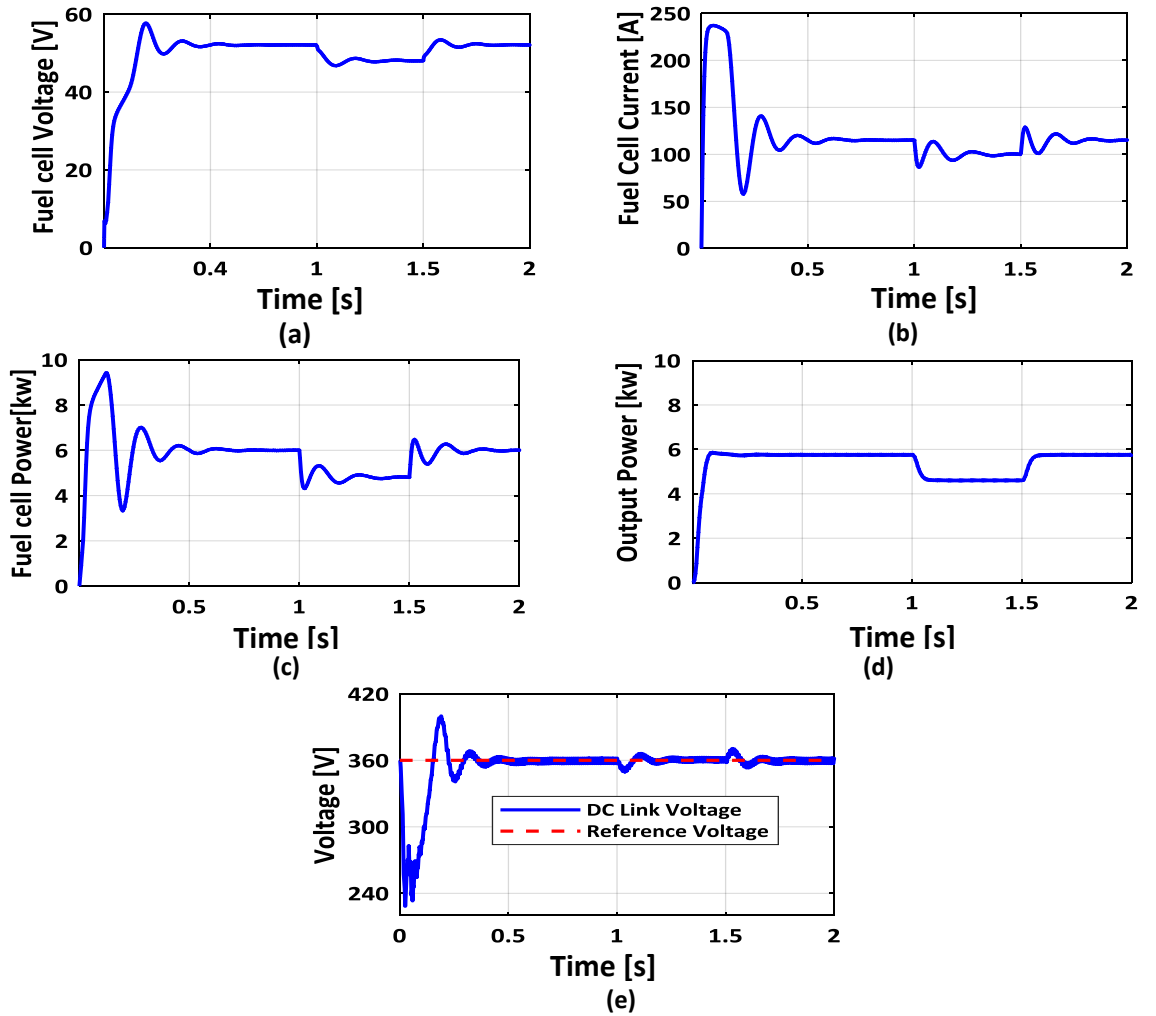


Fig. 16. The fuel cell performance during fuel flow reduction: a) the output voltage; b) the output current; c) the generated power; d) the delivered power; e) DC link voltage.

The grid current quality of the GCFCI-LCL system at different operating points of PEMFC is investigated in Fig. 17. At the full capacity of the fuel cell, the THD of the current on the grid side (i_2) with the proposed control strategy is 1.10%. When the PEMFC operates at its 75% nominal power, the grid current reduces to 75% of its rated value, and its THD is a little increased to 1.5%. Also, when the PEMFC operates at its 50% nominal power, the grid current reduces to 50% of its rated value, and its THD equals 2.26%. According to this investigation, reducing the fuel flow of PEMFC, and consequently, decreasing the power generated by the fuel cell, the THD of injected current to the grid increases insufficiently, while its value is still in the acceptable range of IEEE std. 519.

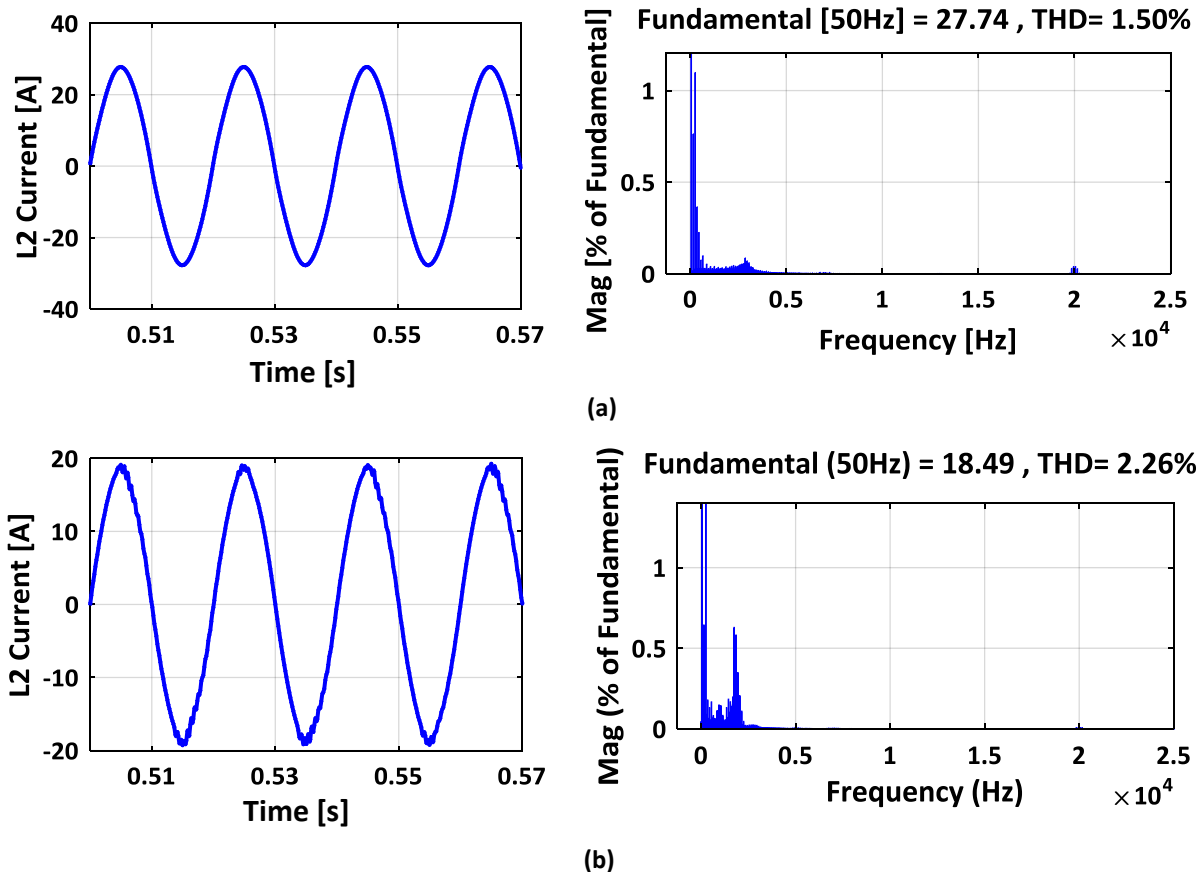


Fig. 17. The grid current waveform and its THD when the fuel flow capacity reduces: a) 25% decrease; b) 50% decrease.

6.4. The Grid Inductance Variation

Usually, the grid impedance is modeled as an inductance series with a resistance. Since this resistance improves the system stability, to investigate the worst condition, only an inductance is considered as the grid impedance. The GCFCI-LCL system operation for the ideal grid and $L_g = 0$ for both the suggested control approach and the traditional active damping, which is based on capacitor current damping, are shown in Fig. 18. For the suggested control strategy, the THD of the inverter side current (i_1) and the grid side current (i_2) is 6.11% and 1.10%, respectively. For traditional active damping method, they are 6.33% and 2.04%, respectively. THD value in the suggested control scheme is lower than the traditional method.

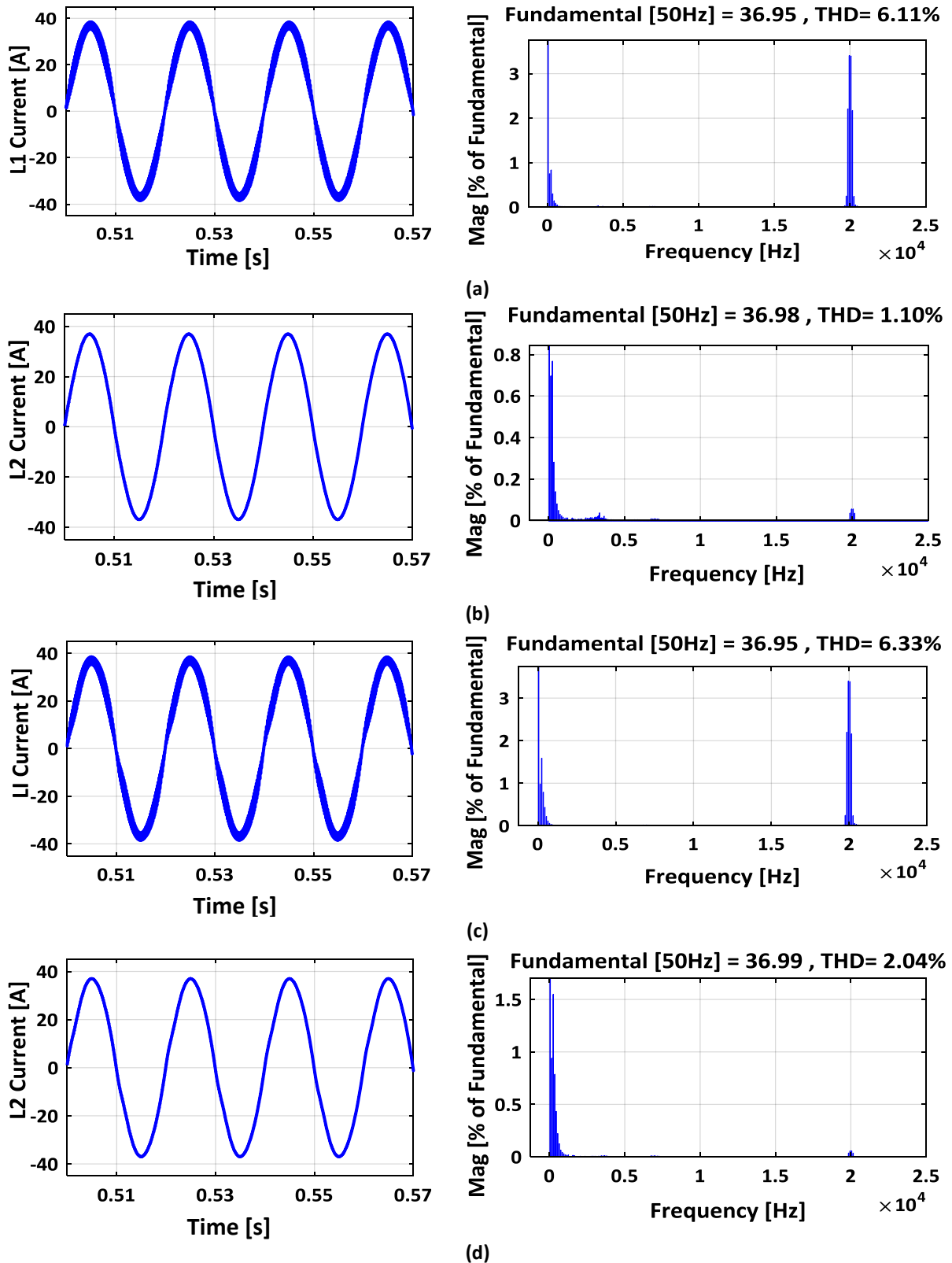


Fig. 18. The grid side current and the inverter side current for $L_g = 0$: a) the inverter side inductance current with the suggested strategy; b) the grid side current with the suggested strategy; c) the inverter side inductance current with the traditional strategy; d) the grid side current with the traditional strategy.

The GCFCI-LCL system operation for the non-ideal grid with $L_g = 4.8mH$ for both the suggested control approach and the traditional active damping are shown in Fig. 19. For the suggested control strategy, the THD of the inverter side current (i_t) and the grid side current

(i_2) is 6.24% and 1.31%, respectively. They are 6.55% and 2.47% respectively for the traditional active damping method. Evaluation of the THD values shows that the quality of the grid side current in the non-ideal grid by the suggested strategy has no remarkable reduction compared with the ideal grid. While, by the traditional method, the quality reduces seriously compared with the ideal grid, which has zero impedance.

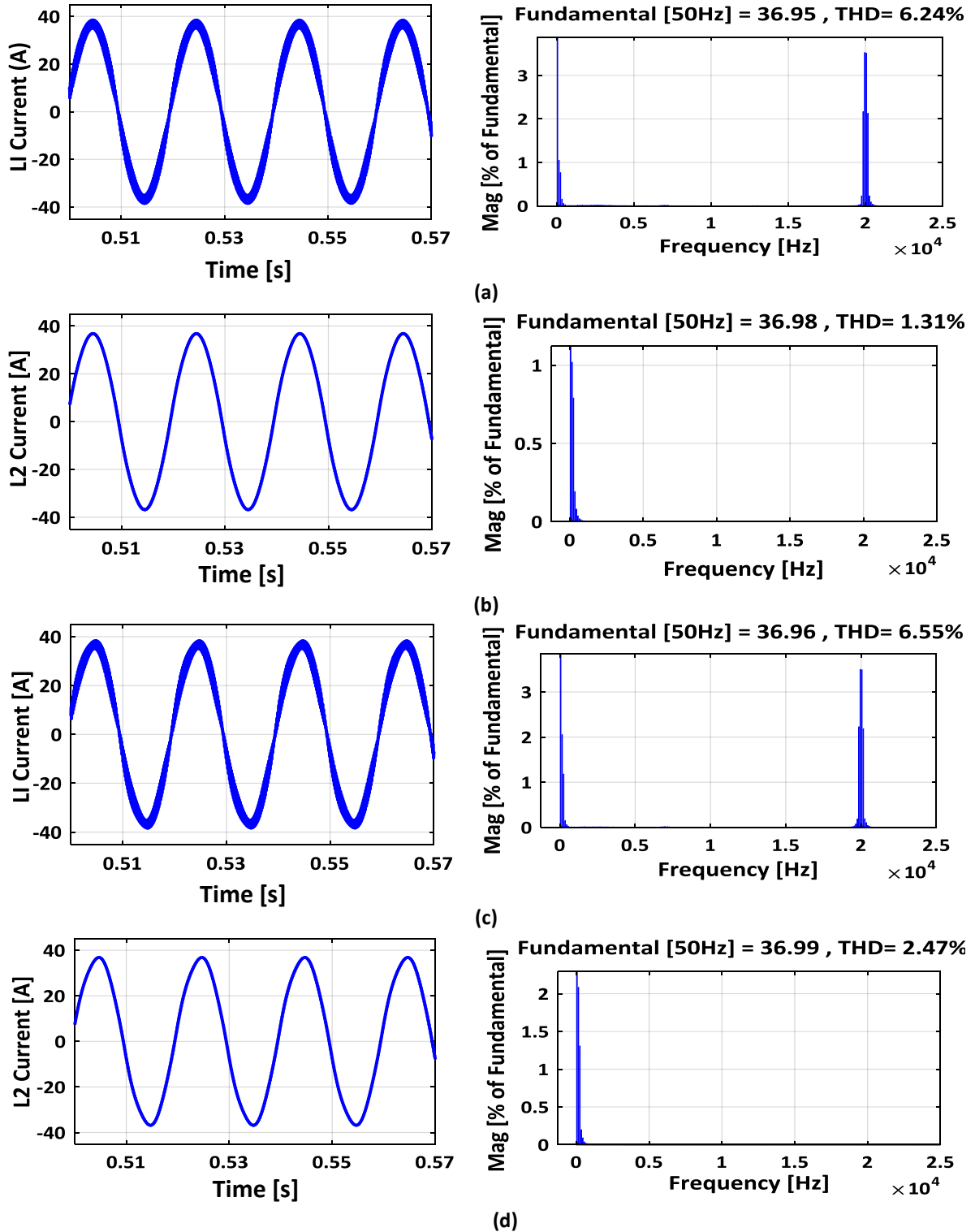


Fig. 19. The grid side current and the inverter side current for $L_g = 4.8\text{mH}$: a) the inverter side inductance current with the suggested strategy; b) the grid side current with the suggested strategy; c) the inverter side inductance current with the traditional strategy; d) the grid side current with the traditional strategy.

At the end of the simulation results, Table 2 presents a comparison between the suggested control method with recent studies about grid-connected power conditioning systems in the weak and harmonic network. As can be seen, the suggested method has a suitable current quality. Stability analysis is carried out in the suggested scheme as well as presented schemes of [14] and [30]. Despite using a Quasi-Y-Source converter in the reference [14], the current quality of the suggested system is somewhat better than [14]. In addition, in the proposed method, contrary to the reference [14], the voltage feed-forward consideration for harmonics-polluted conditions has been carefully investigated. Also, the number of control loops is investigated in Table 2. Some schemes use only one control loop, which results in more uncomplicated control strategy. Some schemes, such as the suggested strategy as well as schemes of [14] and [30], utilize two control loops which results in more complicated strategy. Naturally, in order to achieve better control and higher output quality, a more complex design is justified. It should be noted that the main purpose of presenting Table 2 is not comparing the THD value of similar researches. Presenting several similar studies and their control strategies, utilized filter type, number of control loops and the complexity level of control scheme, presence of stability analysis in weak grid are useful information which is provided through Table 2.

Table 2. Comparison of several control methods with the suggested method.

Applied method	Filter type	Controller	Number control loops	Stability analysis in weak grid	Reported THD
Presented in [29]	LC	Quasi Resonant	2	×	4.5%
Presented in [30]	LCL	PR & Impedance shaping	2	✓	1.27%
Presented in [8]	L	Jaya-Based MPPT	2	×	2.8%
Presented in [31]	LC	VPI	1	×	1.59%
Presented in [32]	LC	Partial feedback Linear controller	2	×	3.97%
Presented in [11]	LC	Active control+VPI	1	×	2.94%
Presented in [33]	Hybrid filter	Backstepping control	2	×	1.89%
Presented in [14]	LCL	PR & CSCF	2	✓	1.21%
Presented in [34]	LC	PR	2	×	2.88%
Suggested	LCL	Inductors' double feedback	2	✓	1.1%

7. CONCLUSIONS

In this paper, an LCL filter was employed to reduce harmonic distortion of the fuel cell generated voltage and current. To achieve LCL filter resonance damping, current double feedback control method - which uses inverter side and grid side currents as feedback current - was used to dampen the resonance and to improve harmonic eliminations. The current regulator parameters were determined based on the Routh-Hurwitz stability criterion. In comparison with the traditional capacitor current active damping strategy, the suggested strategy showed a higher stability margin and lower THD for both the inverter side and the grid side currents. Stability analysis for high variation in the grid inductance and sensitivity

analysis for changing LCL filter inductor values showed proper stability of the system against the grid and the filter parameter variations. The simulation results verified the performance of the suggested strategy for both zero inductance ideal and inductive non-ideal grids. The suggested control strategy performed well in fuel cell power transmission into the grid and showed good dynamical behavior against fuel cell input disturbances.

REFERENCES

- [1] M. Rahimian, A. Dejamkhooy, M. Hosseinpour, A. Yazdian-Varjani, "Efficiency improvement and reliability evaluation of small-scale PMSG-based wind energy conversion system using back-to-back T-type converter," *Electrical Engineering*, vol. 103, no. 6, pp. 2897-2909, 2021.
- [2] N. Rasekh, M. Hosseinpour, A. Dejamkhooy, A. Akbarimajd, "Robust power conditioning system based on LCL-type quasi-Y-source inverter for grid connection of photovoltaic arrays," *International Journal of Automation and Control*, vol. 15, no. 6, pp. 692-709, 2021.
- [3] A. Veerendra, M. Mohamed, P. Leung, A. Shah, "Hybrid power management for fuel cell/supercapacitor series hybrid electric vehicle," *International Journal of Green Energy*, vol. 18, no. 2, pp. 128-143, 2021.
- [4] M. Inci, O. Turksoy, "Review of fuel cells to grid interface: configurations, technical challenges and trends," *Journal of Cleaner Production*, vol. 213, pp. 1353-1370, 2019.
- [5] N. Mebarki, T. Rekioua, Z. Mokrani, D. Rekioua, S. Bacha, "PEM fuel cell/battery storage system supplying electric vehicle," *International Journal of Hydrogen Energy*, vol. 41, no. 45, pp. 20993-21005, 2016.
- [6] C. Wu, J. Chen, C. Cu, Z. Liu, "Real-time adaptive control of a fuel cell-battery hybrid power system with guaranteed stability," *IEEE Transactions on Control Systems Technology*, vol. 25, no. 4, pp. 1394-1405, 2016.
- [7] O. Madani, T. Das, "Feedforward based transient control in solid oxide fuel cells," *Control Engineering Practice*, vol. 56, pp. 86-91, 2016.
- [8] S. Padmanaban, N. Priyadarshi, M. Bhaskar, J. Holm-Nielsen, E. Hossain, F. Azam, "A hybrid photovoltaic-fuel cell for grid integration with Jaya-based maximum power point tracking experimental performance evaluation," *IEEE Access*, vol. 7, pp. 82978-82990, 2019.
- [9] Y. Devrim, L. Bilir, "Performance investigation of a wind turbine-solar photovoltaic panels-fuel cell hybrid system installed at Incek region-Ankara Turkey," *Energy Conversion and Management*, vol. 126, pp. 759-766, 2016.
- [10] M. Banaei, S. Sani, "Analysis and implementation of a new SEPIC-based single-switch buck-boost DC-DC converter with continuous input current," *IEEE Transactions on Power Electronics*, vol. 33, no. 12, pp. 10317-10325, 2018.
- [11] Q. Li, W. Chen, Z. Liu, G. Zhou, L. Ma, "Active control strategy based on vector-proportion integration controller for proton exchange membrane fuel cell grid-connected system," *IET Renewable Power Generation*, vol. 9, no. 8, pp. 991-999, 2015.
- [12] A. Naderipour, A. Zin, M. Habibuddin, M. Mortadi, M. Miveh, H. Afrouzi, "A new compensation control strategy for grid-connected wind turbine and fuel cell inverters in a microgrid," *International Journal of Power Electronics and Drive Systems*, vol. 8, no. 1, pp. 272-278, 2017.
- [13] S. Khajehoddin, M. Karimi-Ghartemani, P. Jain, A. Bakhshai, "DC-bus design and control for a single-phase grid connected renewable converter with a small energy storage component," *IEEE Transactions on Power Electronics*, vol. 28, no. 7, pp. 3245-3254, 2013.

- [14] N. Rasekh, M. Hosseinpour, "LCL filter design and robust converter side current feedback control for grid-connected proton exchange membrane fuel cell system," *International Journal of Hydrogen Energy*, vol. 45, no. 23, pp. 13055-13067, 2020.
- [15] Z. Zhang, W. Wu, Z. Shuai, X. Wang, A. Luo, H. Chung, F. Blaabjerg, "Principle and robust impedance-based design of grid-tied inverter with LLCL-filter under wide variation of grid-reactance," *IEEE Transactions on Power Electronics*, vol. 34, no. 5, pp. 4362-4374, 2019.
- [16] J. Sosa, P. Martinez-Rodriguez, G. Escobar, G. Vazquez, A. Valdez-Fernandez, "Active power injection control for power converters connected to the grid through an L filter," *Electric Power Components and Systems*, vol. 45, no. 6, pp. 660-671, 2017.
- [17] P. Mishra, R. Maheshwari, "Design, analysis, and impacts of sinusoidal LC filter on pulse width modulated inverter fed-induction motor drive," *IEEE Transactions on Industrial Electronics*, vol. 67, no. 4, pp. 2678-2688, 2020.
- [18] M. Hosseinpour, N. Rasekh, "A single-phase grid-tied PV based trans-z-source inverter utilizing LCL filter and grid side current active damping," *Journal of Energy Management and Technology*, vol. 3, no. 3, pp. 67-77, 2019.
- [19] J. Fang, H. Li, Y. Tang, "A magnetic integrated LLCL filter for grid-connected voltage-source converters," *IEEE Transactions on Power Electronics*, vol. 32, no. 3, pp. 1725-1730, 2017.
- [20] N. Rasekh, M. Rahimian, M. Hosseinpour, A. Dejamkhooy, A. Akbarimajid, "A step by step design procedure of PR controller and capacitor current feedback active damping for a LCL-type grid-tied T-type inverter," *In 2019 10th International Power Electronics, Drive Systems and Technologies Conference*, pp. 612-617, 2019.
- [21] C. Chen, J. Xiong, Z. Wan, J. Lei, K. Zhang, "A time delay compensation method based on area equivalence for active damping of an LCL-type converter," *IEEE Transactions on Power Electronics*, vol. 32, no. 1, pp. 762-772, 2017.
- [22] S. Parker, B. McGrath, D. Holmes, "Regions of active damping control for LCL filters," *IEEE Transactions on Industry Applications*, vol. 50, no. 1, pp. 424-432, 2014.
- [23] T. Chen, C. Lee, S. Hui, "A general design procedure for multi-parallel modular grid-tied inverters system to prevent common and interactive instability," *IEEE Transactions on Power Electronics*, vol. 34, no. 7, pp. 6025-6030, 2019.
- [24] J. Yin, S. Duan, B. Liu, "Stability analysis of grid-connected inverter with LCL filter adopting a digital single-loop controller with inherent damping characteristics," *IEEE Transactions on Industrial Informatics*, vol. 9, no. 2, pp. 1104-1112, 2013.
- [25] D. Pan, X. Ruan, C. Bao, W. Li, X. Wang, "Capacitor-current feedback active damping with reduced computation delay for improving robustness of LCL-type grid-connected inverter," *IEEE Transactions on Power Electronics*, vol. 29, no. 7, pp. 3414-3427, 2014.
- [26] J. Yang, F. Lee, "LCL filter design and inductor current ripple analysis for a three-level NPC grid interface converter," *IEEE Transactions on Power Electronics*, vol. 30, no. 9, pp. 4659-4668, 2015.
- [27] Y. Guan, Y. Wang, Y. Xie, Y. Liang, A. Lin, X. Wang, "The dual-current control strategy of grid-connected inverter with LCL filter," *IEEE Transactions on Power Electronics*, vol. 34, no. 6, pp. 5940-5952, 2019.
- [28] D. Pan, X. Ruan, C. Bao, W. Li, X. Wang, "Optimized controller design for LCL-type grid-connected inverter to achieve high robustness against grid-impedance variation," *IEEE Transactions on Industrial Electronics*, vol. 62, no. 3, pp. 1537-1547, 2015.
- [29] C. Lai, Y. Lin, Y. Cheng, L. Yao, "Development of a modular single-phase grid-tie inverter system for fuel-cell power generation," *Journal of the Chinese Institute of Engineers*, vol. 41, no. 2, pp. 112-123, 2018.

- [30] M. Hosseinpour, A. Kholousi, A. Poulad, "A robust controller design procedure for LCL-type grid-tied proton exchange membrane fuel cell system in harmonics-polluted network," *Energy Science and Engineering*, vol. 10, no. 10, pp. 3798-3818, 2022.
- [31] W. Chen, Y. Han, Q. Li, Z. Liu, F. Peng, "Design of proton exchange membrane fuel cell grid-connected system based on resonant current controller," *International Journal of Hydrogen Energy*, vol. 39, no. 26, pp. 14402-14410, 2014.
- [32] S. Mohiuddin, C. Macana, H. Pota, T. Hossen, M. Mahmud, "Nonlinear partial feedback linearizing controller design for grid-connected fuel-cell system with third harmonic injected PWM approach," *In 2017 North American Power Symposium*, pp. 1-6, 2017.
- [33] S. Ankur, M. Narayana, S. Mohanty, N. Kishor, "Power quality improvement in grid-connected photovoltaic-fuel cell based hybrid system using robust maximum power point tracking controller," *Electric Power Components and Systems*, vol. 43, no. 20, pp. 2235-2250, 2015.
- [34] Y. Yang, X. Guo, Z. Lu, C. Hua, M. Castilla, F. Blaabjerg, "Advanced control of grid-connected inverters for proton exchange membrane fuel cell system," *International Journal of Hydrogen Energy*, vol. 45, no. 58, pp. 33198-33207, 2020.